PREDICTION OF THE POINTING STABILITY FROM GROUND TEST AND ITS INITIAL IN-ORBIT EVALUATION OF THE SOLAR OBSERVATION SATELLITE SOLAR-B

O. Takahara(1) , K. Ichimoto(2), T. Shimizu(3), Y. Sakamoto(4), S. Nagata(5), S. Shimada(6) and N. Yoshida(1)
(1)Advanced Technology R&D Center, Mitsubishi Electric Corp., 8-1-1,Tsukaguchi-Homachi, Amagasaki, Hyogo 661-8661, JAPAN
(2) National Astronomical Observatory of Japan, 2-21-1 Osawa, Mitaka, Tokyo, 181-8588, JAPAN
(3) Institute of Space and Astronautical Science, Japan Aerospace Exploration Agency, 3-1-1 Yoshinodai, Sagamihara, Kanagawa 229-8510, JAPAN
(4) University of Tokyo, 2-21-1 Osawa, Mitaka, Tokyo, 181-8588, JAPAN
(5) Kyoto University, Hida Observatory, Kurabashira, Kamitakara-cho, Takayama, Gifu, 506-1314, JAPAN
(6) Kamakura Works, Mitsubishi Electric Corp., 325, Kamimachiya, Kamakura, Kanagawa, 247-8520, JAPAN

ABSTRACT

The SOLAR-B ('HINODE') is a Japanese solar observation satellite that was developed jointly with the US and UK. It carries three telescopes and was successfully launched in September 2006. Among the three telescopes, the Solar Optical Telescope (SOT) requires the highest pointing stability of 0.03 arcseconds (1 sigma) in 10 seconds.

The greatest issue in achieving pointing stability is microvibration that was generated by dozens of disturbance sources inside the satellite, such as momentum wheels, mechanical gyros, mechanical shutters and filter wheels. Even the vibration of 10^{-6} g level may cause relative movements of optical elements of the telescopes that induce pointing error well exceeding the requirement. To predict the performance of SOT from ground test, the inertial and optical measurement methods were adapted. And the effects of the launch vibration and thermal environment on the pointing stability, was evaluated.

This paper presents the method of optical measurement and the prediction results from the test. In addition, the initial in-orbit evaluation of the satellite performance is described.

1. INTRODUCTION

The SOLAR-B ('HINODE') is a solar observation satellite that was launched on September 23, 2006. The satellite was developed by the Institute of Space and Astronautical Science of Japan Aerospace Exploration Agency (ISAS/JAXA) and National Astronomical Observatory of Japan (NAOJ) with the US and UK teams. The in-orbit configuration of SOLAR-B is shown in Figure 1.

There are three onboard telescopes, the Solar Optical Telescope (SOT), the X-Ray Telescope (XRT), and the Extreme Ultra-Violet Imaging Spectrometer (EIS). These were developed by international teams; a Japan-US team is responsible for SOT, a UK-US-Japan team for EIS and a US-JAPAN team for XRT. Mitsubishi Electric Corporation (MELCO) supports system design and integration of S/C bus and OTA. The highest pointing stability required for SOT, is 0.03 arcseconds (1 sigma)[1].

One of the biggest problems in satisfying required level of pointing stability, is microvibration arising from Attitude and Orbit Control Subsystem (AOCS) components, such as mechanical gyroscopes, momentum wheels (MW's), and moving components within telescopes.

It is almost impossible to precisely evaluate the pointing error induced by microvibration based on the analysis with the finite element method, because the structural damping is not exactly known, and eigenmodes and eigenfrequencies are inaccurate in higher modes. Therefore, measurement is the only method to evaluate the pointing error in high frequency region. However, in this measurement, environmental and electrical noise is one of the biggest problem, because the vibration level to be measured is very small, and certain techniques are required to reduce the noise.

In the early development phase of SOLAR-B, the

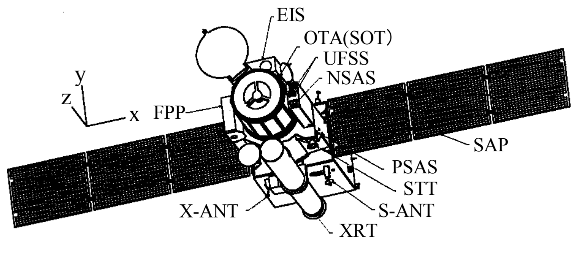

Figure 1 In-orbit configuration of SOLAR-B

disturbance level of all major sources and the transmissibility from disturbance sources to pointing errors of telescopes were evaluated separately by measurement. In the transmissibility measurement, the inertial sensors with high sensitivity were used. The pointing stability of SOT was estimated with these data. [2]

In the final phase, the end-to-end measurement of pointing stability of SOT based on optical method, was performed by actually exciting major disturbance sources. In addition, the measurement was executed before and after vibration test and also after thermal-vacuum test in order to evaluate the influence of the launch vibration and thermal environment on the pointing stability.

2. DISTURBANCE SOURCES

There are various internal disturbance sources in SOLAR-B, and their frequency range, level and waveform are different. They are grouped into two categories, steady-state disturbance and non steady-state disturbance, as shown in Table 1. The steady-state disturbance sources are AOCS components such as four MW's and three mechanical gyro units. They always rotate at a certain velocity. The non steady-state disturbance sources are filter wheels, shutters and so on, installed in three telescopes, and move intermittently.

Table 1 Major disturbance sources in Solar-B

Disturbance classification	Equipment	Moving components
Steady-state	AOCS	MW
		IRU-SA(*1)
		IRU-B1,IRU-B2(*2)
Non steady-state	FPP	・NFI Filter Wheel ・BFI Filter Wheel etc.
	XRT	・Filter Wheel 1 ・Filter Wheel 2 etc.
	EIS	・Slit Mechanism ・Shutter Mechanism etc.

(*1) IRU-SA: sensor assembly of IRU-A (FRIG)
(*2) IRU-B1,B2: Unit #1 & #2 of IRU-B
(Tuned Dry Gyro)

3. MEASUREMENT METHOD TRADE-OFF

In measuring pointing error induced by microvibration, to select measurement method and boundary condition is important. There are two methods: One is the optical measurement method, and the other is the inertial measurement method. The optical method is to measure the jitter of the mission sensor light axis optically by injecting collimated light from an outside light source. The jitter was actually detected by two methods. One is the direct measurement of movement of the light source image on the focal plane of the mission sensor. The other is to extract the injected light by a beam splitter set between the OTA and the Focal Plane Package (FPP). On the other hand, the inertial method is to measure the mission sensor light axis indirectly by detecting the translational and rotational movements of major optical elements of the mission sensor, and then by converting these movements to the pointing jitter. As many as fifteen inertial sensors were put on the main mirror and the sub mirror.

Each method has advantages and disadvantages in evaluating the pointing error.

As for the optical measurement method, the biggest advantage is to measure pointing error directly. A major disadvantage is that the boundary condition is restricted to a fixed-free configuration because it is required to keep the angle between the optical axis of a mission sensor and that of light source constant. In this boundary condition, background noise in signal increases substantially, because seismic vibration of the building is transmitted to the mission sensor and the light source, and the relative angle between the injected light and the optical axis of the mission sensor are affected. Therefore how to reduce the noise is very important in the data analysis. In addition, the resonance frequencies and global mode shapes for the fixed-free condition are different from those for the free-free boundary condition in orbit.

In the inertial measurement method, the boundary condition is not restricted, and both fixed-free condition and free-free condition can be used. The free-free condition is thought better to simulate the in-orbit boundary condition. The free-free condition is realized by either hanging a satellite via springs from the ceiling of the test room or setting it on soft material[2],[3],[4]. An additional benefit of this boundary condition is the ability of cutting off the low frequency noise coming from the floor and ceiling. The first disadvantage is the inability of evaluating pointing error directly. The second one is the risk of contaminating the mission sensor because it is indispensable to mount inertial sensors on optical components of the mission sensor.

In the early development phase of the Solar-B, the pointing errors were evaluated based on the different boundary conditions and measurement methods, and the results were compared through experiment. The inertial measurement with the inertial sensors on the main mirror and the sub mirror was conducted both in free-free and fixed-free configurations, and the pointing errors were almost identical. The reason is thought to be as follows; the frequencies of disturbances present in the SOLAR-B are higher than 100Hz and in this region global modes are not greatly excited. Next, the pointing errors evaluated by the optical method and the inertial method were compared using the same fixed-free condition. The evaluation results approximately coincided, although the optical method gave one order higher pointing error without background noise reduction. The remaining

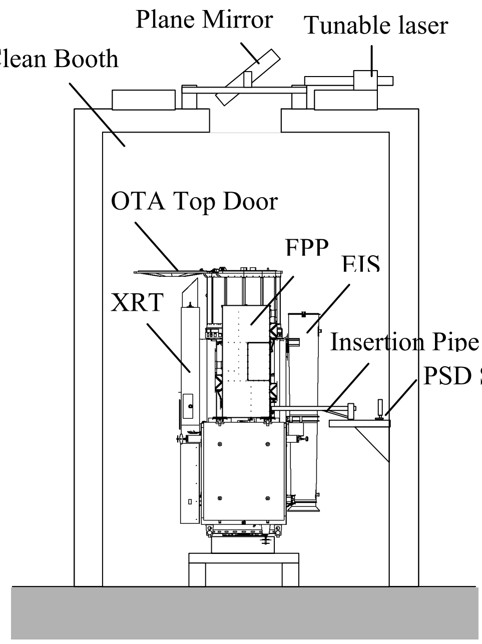

Figure 2 Test configuration for the optical measurement

difference was attributed to (1) limited locations of sensors in the inertial measurement (only on the main mirror and the sub mirror), and (2) the remaining noise especially in the optical measurement induced by the vibration of the light source and the detection sensor.

In the FM test of Solar-B, the optical measurement method with fixed-free boundary condition was adopted in order to avoid contaminating the mission sensor.

4. TEST METHOD AND CONDITION ON GROUND TEST

4.1. Test configuration

The test configuration is shown in Figure 2. The fixed-free configuration and the optical measurement method were adopted. The satellite was put on the dolly with solar array paddles folded, was put inside a clean booth covered with plastic sheets. Laser beam source, which is a tunable laser, is set on the top of the clean booth. The collimated laser beam was projected into the

Table 2 Condition of microvibration test

Disturbance source	Driving condition
IRU-SA	Rotation at a fixed speed
IRU-B1,-B2	Rotation at a fixed speed
IRU-SA +four MW's	IRU-SA: Rotation at a fixed speed MW: One wheel rotates with the speed slowly varied and others rotate at a fixed speed
Moving components in FPP, EIS, XRT	Continuous movement or Single movement

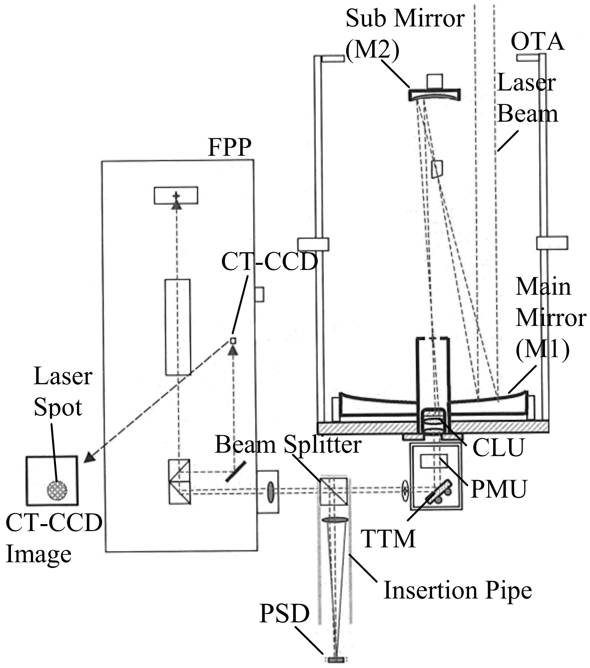

Figure 3 Optical layout and optical measurement system of SOT

optical system of SOT after being reflected by a plane mirror. Four acceleration sensors were set on four locations: the top of the clean booth, the laser light source, the plane mirror, and the floor. Three tests with the identical configuration were executed at ISAS/JAXA.

4.2. Optical measurement system

The optical layout and the optical measurement system of SOT are shown in Figure 3. The SOT consists of the OTA and the FPP. The beam splitter is inserted in the optical path between the OTA and the FPP for the test.

The pointing error was evaluated by the position sensitive detector (PSD) and the CCD sensor, and the evaluated values were compared. The PSD detects the position jitter of the laser source seen from the OTA. The CCD also detects the position jitter of the laser source through the OTA and the FPP. The Correlation Tracker (CT), that is used to track the sun's surface on orbit, was used to detect the pointing jitter in this test. The image-based pointing control called CTM (the Correlation tracker and the Tip-tilt Mirror) inside the FPP was operated during the test, but it does not affect the pointing jitter since the disturbance frequencies are higher than the control bandwidth of the CTM. The sampling rates of PSD and CTM-CCD are 3 kHz and about 600 Hz, respectively.

4.3. Test condition

The data was acquired with various disturbance sources actually driven individually. The drive conditions of the disturbance sources are shown in Table 2. The wheel speed of the MW was slowly swept from 1700 rpm to 1900 rpm. This range was decided based on the results of the previous test in order to minimize the pointing error caused by the MW disturbance. The components in the FPP, EIS and XRT were operated in typical operating condition in orbit.

To avoid the noises coming from the floor and ceiling, air-conditioning in the clean room, the clean booth and other nearby facilities were stopped.

4.4. Data analysis method

The data analysis method was carefully selected depending on the disturbance types. An important point to be considered is the reduction method of the background noise, since the signal level induced by disturbances is very low in most cases.

4.4.1. Analysis of pointing error by steady-state disturbances

The pointing error $\Delta\theta_i(f_j)$ is calculated according to Equation (1).

(1) $$\Delta\theta_i(f_j) = \sqrt{P_i(f_j) - P_{(BG)i}(f_j)}$$

$$\Delta\theta_i(f_j) = 0 \quad \text{when} \quad P_i(f_j) - P_{(BG)i}(f_j) \le 0,$$

where i is the optical axis of an optical system, (1:about x, 2: about y), f_j is the center frequency for j^{th} frequency band, $P_i(f_j)$ is the power spectrum of the pointing error with disturbance source driven, and $P_{(BG)i}(f_j)$ is the power spectrum with disturbance source not excited. It was assumed that the statistical property of background noise does not change with time. The pointing error caused by the disturbance sources except MW's (e.g., gyro) was calculated, using Equation (2) in dominant frequencies, which were determined by measuring the disturbance source.

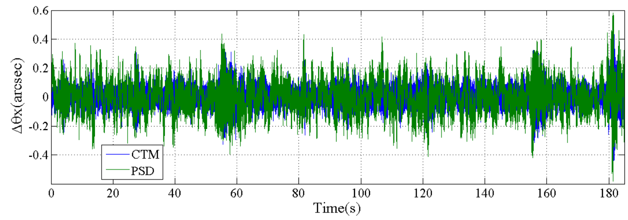

Figure 4 Raw data of the pointing error by the FPP BFI Filter wheel

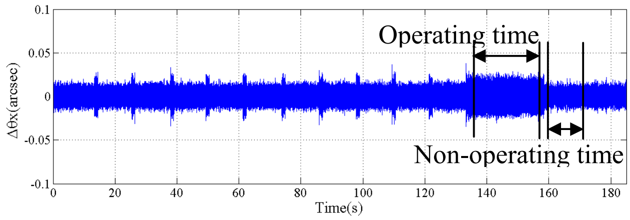

Figure 5 Filtered data of the pointing error by the FPP BFI Filter wheel with PSD sensor

(2) $$\Delta\theta_i = \sqrt{\sum_j \{\Delta\theta_i(f_j)\}^2}$$

As for the pointing error $\Delta\theta_i(f_j, n)$ caused by MW's, the disturbance spectrum varies with wheel speed so that the evaluation is based on Equation (3).

(3) $$\Delta\theta_i(f_j, n) = \sqrt{P_i(f_j, n) - P_{(BG)i}(f_j)}$$

$$\Delta\theta_i(f_j, n) = 0 \quad \text{when} \quad P_i(f_j, n) - P_{(BG)i}(f_j) \le 0,$$

where n is the wheel speed, $P_i(f_j, n)$ is the power spectrum of the pointing error. In evaluating $P_i(f_j, n)$, the data were divided into a series of data for a short time period within which the wheel speed is assumed to be constant. To see the dependence of the pointing error on the wheel speed, Equation (4) was used.

(4) $$\Delta\theta_i(n) = \sqrt{\sum_j \{\Delta\theta_i(f_j, n)\}^2}$$

Here the disturbance caused by MW's includes lots of frequency components, and the summation has to be taken over the frequency range of interest.

4.4.2. Analysis of pointing error by non steady-state disturbances

Background noise level is so high, as shown in Figure 4, that the pointing error by non steady-state disturbance sources is hardly distinguished. The following techniques were used to reduce the noise.

1) Filter out the background noise with a narrow band pass filter with the center frequency at the disturbance frequency to be analyzed.
2) Separate data for operating time and that for non-operating time (Figure 5)
3) Evaluate the power spectra for the operating time and the non-operating time, respectively.
4) Calculate the total pointing error, using equations (1) and (2), where the power spectrum for the non-operating time was assumed to be that of background noise.

5. RESULT ON GROUND TEST

5.1. Background noise in the test

The power spectrum of background noise on $\Delta\theta_x$, is shown in Figure 6. The background noise data was acquired with the air conditioners off in the clean room, clean booth, and so on. Since disturbance sources of interest exist in the frequency region higher than 50Hz,

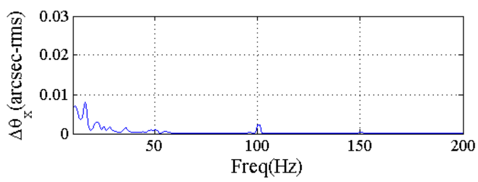

Figure 6 Power spectrum of Background noise

the background noise is low enough to evaluate the pointing error induced by disturbance sources.

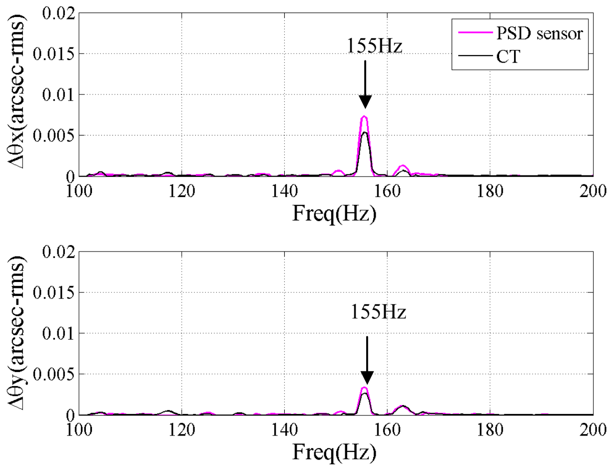

Figure 7 Power spectrum of pointing error by IRU-B, IRU-B2

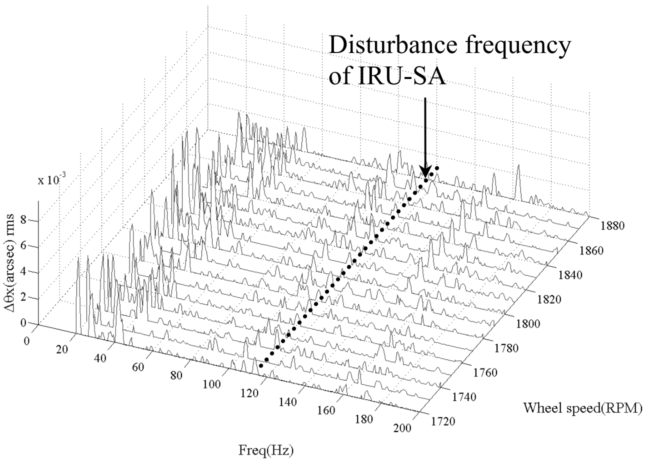

Figure 8 Water fall plot
(MWA: 1900 rpm→1700 rpm, MW-B,-C,-D: 1900 rpm)

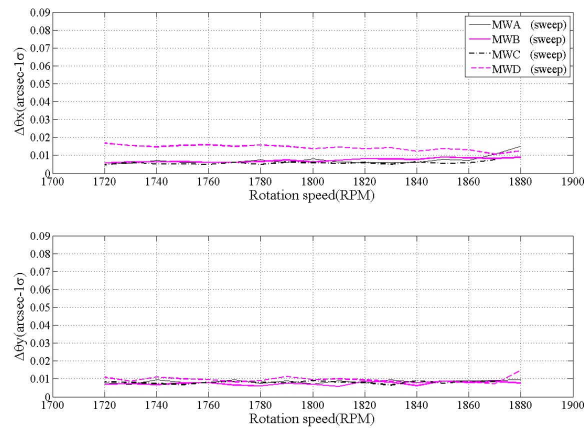

Figure 9 MW wheel speed vs. pointing stability after thermal vacuum test

5.2. Pointing error caused by IRU-B1 and IRU-B2

The power spectra of pointing error by two sensors, PSD sensor and CTM-CCD, are shown in Figure7, while IRU-B1 and IRU-B2 are driven. It is confirmed that the disturbance frequency is 155 Hz. Also, the magnitude of the pointing error at this frequency almost coincides for the measurement results by the two sensors. The result indicates that the disturbances affect mainly optical elements in OTA, but not those in the FPP.

5.3. Pointing error with MW's and IRU-SA driven

The waterfall plot of the spectrum of pointing error by MW's and IRU-SA, is shown in Figure 8. The wheel speed of MW-A was swept from 1900 rpm to 1700 rpm, while those of the other MW's are fixed to a constant speed. IRU-SA was also driven simultaneously. The spectrum was based on the data measured by PSD.

The components of pointing error in the lower frequency region (<50Hz), were caused by the background noise during the measurement as is show in Figure 6. The pointing error due to IRU-SA did not depend on the wheel speed and is almost constant both in magnitude and frequency (114Hz). The pointing error components beyond 50Hz other than 114Hz were considered to be induced by the MW's. The pointing error due to MW's were evaluated from 50 to 200Hz using Equation (4).

The changes of the pointing error vs. the wheel speed of each MW are shown in Figure 9. The pointing error is almost constant in the range of wheel speed of 1700 -1900rpm, and is 0.02 arcseconds or less.

5.4. Pointing error by non steady-state disturbances

As an example, the power spectrum of the pointing stability by the FPP Filter Wheel, is shown in Figure 10. This disturbance mainly comes from a torque ripple of the stepping motor during the operation. The pointing error caused by the transient disturbance during the start and stop operation turned out to be small compared to the error by the torque ripple. It was observed that the dominant frequency of the disturbance is 114±2Hz. The pointing error was evaluated in this frequency range using Equation (1) & (2). The pointing error $\Delta\theta_x$ and $\Delta\theta_y$ are 0.0024 arcseconds (1 sigma) and 0.0092 arcseconds (1 sigma), respectively. They were less than the allocated level, which is 0.01arcseconds (1 sigma). The measured results of the pointing error by major non steady-state disturbance sources are shown in Table 3. The pointing error by certain components such as the visible light shutter is greater than the required level. However, they are scarcely used in orbit so that the contribution was not included in the evaluation of the total pointing error caused by all disturbance sources.

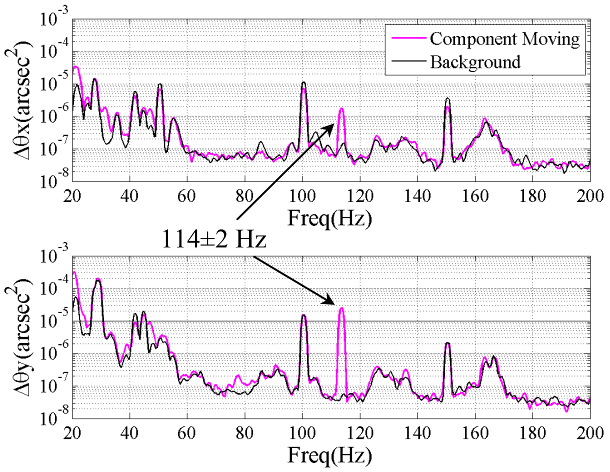

Figure 10 Power spectrum of pointing error of FPP NFI Filter Wheel. Comparison between moving condition vs. non-operating condition after thermal vacuum test

5.5. Pointing stability prediction of SOT

The pointing stability $\Delta\theta_{i,ALL}$ of SOT is evaluated according to Equation (5).

(5) $$\Delta\theta_{i,ALL} = \sqrt{\Delta\theta_{i,S}{}^2 + \Delta\theta_{i,T}{}^2},$$

where $\Delta\theta_{i,S}$ is the sum of the pointing errors by all steady-state disturbance sources, and $\Delta\theta_{i,T}$ is the sum of the pointing stability by non steady-state disturbance sources.

The evaluation results of the pointing stability, before and after vibration test, and after thermal-vacuum test are shown in Figure 11. The steady-state disturbance sources are dominant for the total pointing stability for SOT. From this figure, it was estimated that the launch vibration and thermal environment would not greatly affect the pointing stability. The figure also shows the total pointing stability $\Delta\theta_x$ and $\Delta\theta_y$ is better than the required level of SOT, which is 0.09 arcseconds (3 sigma), or equivalently, 0.03 arcseconds (1 sigma)

Table 3 Pointing error caused by major non steady-state disturbance after thermal vacuum test

Equipment	Moving component	$\Delta\theta_x$ (arcseconds-1 sigma)	$\Delta\theta_y$ (arcseconds-1 sigma)
FPP	NFI Filter Wheel	0.0024	0.0092
	BFI Filter Wheel	0.0020	0.0084
	NFI Mask Wheel (*3)	0.0008	0.0037
	BFI Shutter(*3)	0.0027	0.0019
	NFI Shutter(*3)	0.0017	0.0013
XRT	Filter Wheel 1	0.0035	0.0148
	Filter Wheel 2	0.0037	0.0119
	Visible Light Shutter	0.0461	0.0437

(*3) : Data acquired at the previous tests

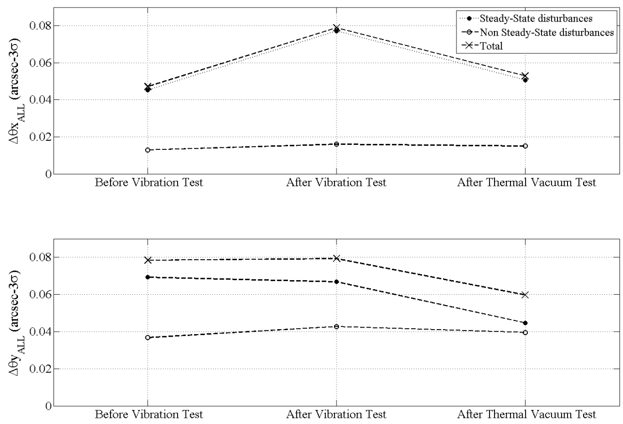

Figure 11 Change of pointing stability throughout two environmental tests

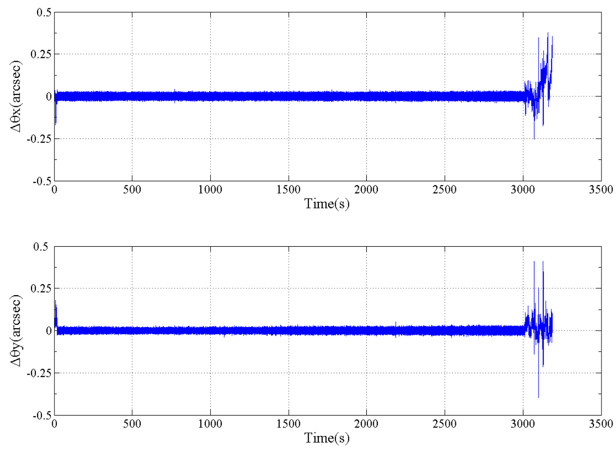

Figure 12 Initial in-orbit pointing stability $\Delta\theta_x$, $\Delta\theta_y$

6. INITIAL IN-ORBIT EVALUATION

The pointing errors $\Delta\theta_x$ and $\Delta\theta_y$ acquired by CTM-CCD during the initial in-orbit check-out are shown in Figure 12. The pointing errors $\Delta\theta_x$ and $\Delta\theta_y$ were 0.0094 arcseconds (1 sigma) and 0.0075 arcseconds (1 sigma), respectively. Based on the evaluation result, it was confirmed that the pointing stability satisfies the requirement for SOT. And the pointing stability predicted from the ground test (Figure 11) approximately agreed with the in orbit stability.

The pointing stability from 0 to 3000 seconds, while the CTM is activated, is much better than that after 3000 seconds, during which the CTM is not activated. These results indicate that the CTM is functioning very effectively in reducing the pointing error in orbit.

7. CONCLUSION

The method of evaluating pointing stability at ground by an optical measurement with a laser beam was established. Under the condition that the disturbance sources were driven, pointing stability was evaluated with this method, and it was predicted that the pointing stability satisfies the requirement for SOT. The prediction was confirmed by the initial in-orbit evaluation result.

8. REFERENCE

[1] Norimasa Yoshida et al., "Systematic Approach to Achieve Fine Pointing Requirement of SOLAR-B", Proceedings of IFAC ACA2004 (16th Symposium on Automatic Control in Aerospace), St-Petersburg, Russia, June, 2004

[2] Osamu Takahara et al., "Microvibration Transmissibility Test of Solar-B", Proceedings of the 24th International Symposium on Space Technology and Science, Miyazaki, Japan, May, 2004

[3] Michel Privat, "On ground and in orbit microvibrations measurement comparison", Proceedings of the 8th European Space Mechanisms and Tribology Symposium, Toulouse, France, pp.181-186, September, 1999

[4] C. Galeazzi, et al., "Experimental Activities On Artemis for The Microvibration Verification", Proceedings of conference on Spacecraft Structure, Materials & Mechanical Testing, Noordwijk, The Netherlands, pp.997-1006, March, 1996